

Poludnista Dorsa, Venus: History and context of a deformation belt

D. A. Young and V. L. Hansen

Department of Geological Sciences, University of Minnesota at Duluth, Duluth, Minnesota, USA

Received 18 April 2004; revised 29 August 2004; accepted 22 October 2004; published 5 March 2005.

[1] Rolling lowlands comprise 80% of Venus's surface, and thus developing a geological understating of resurfacing and tectonism is critical for our understanding of Venus' evolution. In this paper, global, regional, and local approaches to interpreting Magellan synthetic aperture radar and altimetry radar data are used to constrain modes of lowland evolution, convection processes, and lithospheric structure. Detailed geologic mapping is combined with altimetry data test models of deformation belt evolution in Venus's lowlands. Poludnista Dorsa, a complex 2000-km-long deformation belt, is highly segmented and broadly time transgressive. Long-wavelength deformation is spatially independent of local short-wavelength deformation within the deformation belt and temporally predates regional deformation marked by wrinkle ridges. A mechanically layered lithosphere of regional extent is not required by the local geologic history; local lithospheric thinning or progressive regional thickening of the mechanical layer better explains the observed sequence of events.

Citation: Young, D. A., and V. L. Hansen (2005), Poludnista Dorsa, Venus: History and context of a deformation belt, *J. Geophys. Res.*, *110*, E03001, doi:10.1029/2004JE002280.

1. Introduction

[2] Although strain is generally limited in Venus's lowlands, concentrated zones of deformation do occur as linear belts of ridges and fractures. These deformation belts were first identified on Venus by the Venera 15 and 16 mapping missions [Basilevsky and Head, 1988]. They typically superpose 1-km-wide ridges, interpreted as folds and grabens, on 100-km-scale-wide, 1-km-high warps that can extend for several thousand kilometers [Frank and Head, 1990]. Venus lacks a global tectonic architecture similar to that recognized on Earth, in which intense deformation focuses along relatively narrow plate boundaries. Instead, tectonic features on Venus tend to be low in magnitude and regional in extent. Deformation belts are of considerable interest because they indicate limited horizontal movement within Venus's lithosphere, requiring detailed geological mapping to constrain their diversity and evolution.

[3] Deformation belts are typically associated with planitiae, broad topographic basins thousands of kilometers across and up to a couple of kilometers deep. Gravity/topography ratios indicated that many planitiae are primarily supported by ongoing cold mantle downwellings [Simons *et al.*, 1997; Lawrence and Phillips, 2003]. The two greatest concentrations of deformation belts on Venus are spatially associated with Lavinia Planitia and Vinnara Planitia. Other expressions of lowland tectonism include regional suites of sinuous, presumably fault-related features called wrinkle ridges [McGill, 1993], arrays of parallel

lineaments likely representing fractures [Banerdt and Sammis, 1992; Balme *et al.*, 2004] or dikes [Grosfils and Head, 1994], and circular to quasi-circular tectono-magmatic features hundreds of kilometers in diameter [Stofan *et al.*, 1992] termed coronae.

[4] Given the great length of some arrays of deformation belts, the apparent periodic occurrence, and the prominence of warp-like morphologies at various scales, Zuber [1987a, 1987b, 1990] proposed that deformation belts form as harmonic buckling instabilities driven by regional compression, likely impelled by the coupling of large-scale mantle convection with the lithosphere. Some unresolved problems with this model include evidence for localized volcanic activity within deformation belts [e.g., Sukhanov and Pronin, 1987; Kryuchkov, 1990; Addington, 2001; Young *et al.*, 2002; McGill, 2003], evidence for orthogonal deformation belt trends [Squyres *et al.*, 1992], and evidence for superposed extension and contraction [Squyres *et al.*, 1992; Phillips and Hansen, 1994; Rosenberg and McGill, 2002].

[5] One critical issue concerns the presence of superposed length scales of deformation. Early models assumed that Venus's high surface temperature would greatly weaken the lower crust, resulting in decoupling of the upper crust from the lithospheric mantle [Zuber, 1987a, 1987b, 1990]. This assumption led to predicted simultaneous development of two length scales of deformation [Zuber, 1987b, 1990]. Although Venera imagery (and higher-resolution Magellan imagery) revealed two length scales of deformation, the relative timing of their development is unconstrained, though it is required to be simultaneous for the Zuber model. Given the apparently basaltic nature of surface rocks and an extremely dry atmosphere, anhydrous diabase is

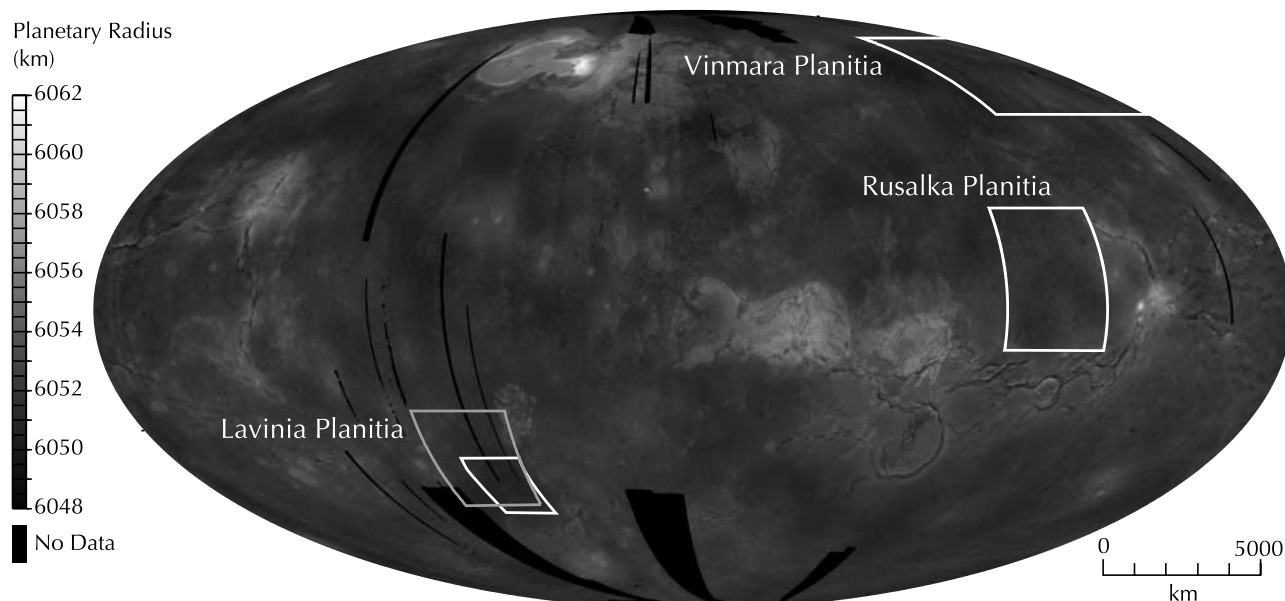


Figure 1. Mollweide projection of Venus topography (Global Topography Data Record (GTDR)) indicating areas of studied deformation belts (Mollweide projection). Vinmara Planitia [Rosenberg and McGill, 2002] and Lavinia Planitia (Squyres *et al.* 1992) (white boxes) and Ivanov and Head [2001] (gray boxes) contain high concentrations of previously studied deformation belts; deformation belts within Rusalka Planitia (Figure 2) are the focus of this investigation.

used for a proxy for Venus's crust. Flow laws for dehydrated Columbia diabase [Mackwell *et al.*, 1998] imply that Venus's crust is very strong, reducing the likelihood of a substantial weak lower crustal layer capable of allowing crustal decoupling [Phillips *et al.*, 1997]. Thus it is important to revisit the question of deformation belt formation in light of new rheological constraints and to evaluate the temporal evolution of deformation belts using high-resolution Magellan mission data.

[6] Did long- and short-wavelength features form synchronously during a relatively punctuated event, or do they record progressive deformation through time and record an extended evolution? Deformation belts could simply be long exposed kipuka, reflecting strong pervasive regional deformation that was later partially obscured by extensive resurfacing processes. Alternatively, deformation belts could reflect fundamentally local processes that later serve as potential "strain magnets" in later tectonic environments. In other words, tectonic spacing recorded by ridge belts may be the result of preservation, initial formation, or some combination of these processes.

[7] In an attempt to address these questions we report on the regional context, detailed geology, and geological history of a previously unstudied deformation belt in Rusalka Planitia, and we survey other features in the region that may provide context. Previously studied deformation belts (Figure 1) occur in Lavinia Planitia (centered at 345°E, 45°S [Squyres *et al.*, 1992; Ivanov and Head, 2002]) and Vinmara Planitia (centered at 195°E, 60°N [Rosenberg and McGill, 2002; McGill, 2003]). Because Rusalka Planitia lay under Magellan's periapsis, the spatial resolution of Magellan radar data at this location exceeds that available for Lavinia and Vinmara planitiae. We find that long- and short-wavelength folds forming the deformation belt formed

diachronously and likely reflect a change in the regional strain field through time. Evidence of local volcanic activity synchronous with deformation belt evolution also indicates that high local heat flow accompanied belt-forming processes.

2. Background

[8] Rusalka Planitia, which lies north of eastern Aphrodite Terra (Figure 1), includes several examples of localized lowland deformation, including graben-dominated kipuka (e.g., Urutonga Colles and Lumo Dorsa), ridge-dominated deformation belts (e.g., Oya Dorsa and Poludnista Dorsa), linear belts that weave around coronae, and long-wavelength warps (e.g., Vetsorgo Dorsum) (Figure 2). Although a deep apparent depth of compensation has not been confirmed directly for Rusalka Planitia because of low-gravity data resolution and the strong signal of nearby topographic highs, the similarity of Rusalka Planitia's size to other planitiae implies that it likely represents a region above contemporary mantle downwelling [e.g., Simons *et al.*, 1997]. Llorona Planitia, similar to Rusalka, lies to the northwest. DeShon *et al.* [2000] discuss the geology of Vetsorgo Dorsum (prior to that feature being named) (area 1 in Figure 2); Young and Hansen [2003] discuss regional geological relations of the other features. This paper focuses on detailed geology of Poludnista Dorsa and Oya Dorsa (area 2 in Figure 2) and attempts to place them in a regional context. Poludnista Dorsa extends ~2000 km along the 180th meridian between Rusalka Planitia and the volcanic highland Atla Regio (area 3 in Figure 2). Oya Dorsa lies on the eastern edge of Llorona Planitia.

[9] Rusalka and Llorona Planitiae record strain at several scales. Wrinkle ridges form a diffuse regional network.

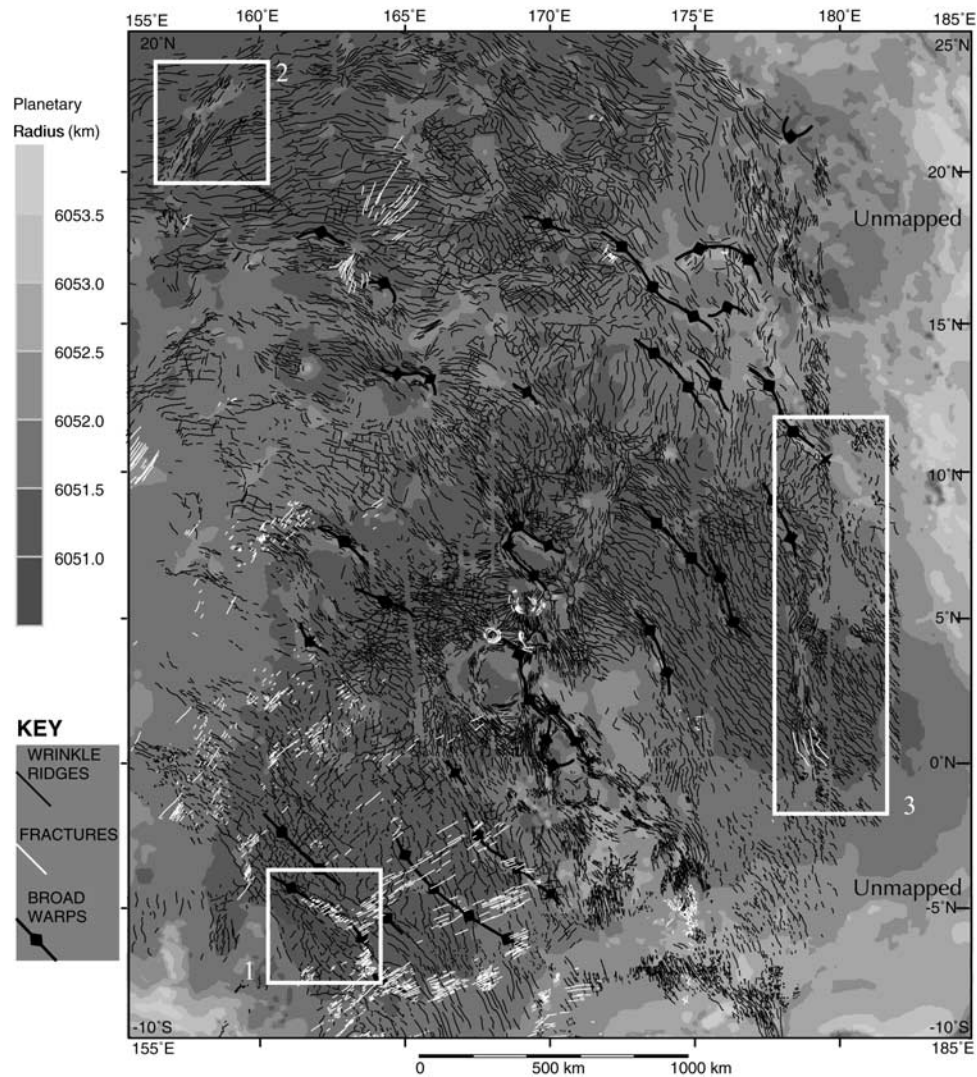


Figure 2. Structural and topographic map of eastern Rusalka Planitia and Llorona Planitia (Mercator projection). A suite of coronae (center) complicates the interior of Rusalka Planitia. The pattern of the wrinkle ridges is complex but generally describes an arc around a center point southwest of the map area. Broad warps trend NW and follow the same general pattern. Area 1 indicates Vetsorgo Dorsum, area 2 indicates Oya Dorsa, and area 3 indicates Poludnista Dorsa (see Figure 3). Data are compiled from *Young and Hansen* [2003], *Hansen and DeShon* [2002], and this study. Topography is from GTDR.

Local suites of parallel lineaments, generally trending perpendicular to the wrinkle ridges, may represent fractures or dikes. Together wrinkle ridges and fracture suites may be interpreted in terms of a consistent overall regional strain ellipse, integrated over time. Locally, more complex deformation associated with coronae and deformation belts is embedded within the regional fabric.

[10] Wrinkle ridges are narrow (~ 1 km), long (tens to hundreds of kilometers), high-backscatter sinuous features that by analogy with similar features on the Moon, Mars, and Mercury are thought to represent limited contractional failure of the lithosphere due to regionally imposed compressional stresses [e.g., *Watters*, 1992; *McGill*, 1993]. *Sandwell et al.* [1997] proposed that the swell-push force generated by contemporary long-wavelength geoid anomalies explains regional wrinkle ridge patterns preserved on Venus [*Bilotti and Suppe*, 1999]. Rusalka Planitia was a

notable exception to this hypothesis; although wrinkle ridges by and large form a regional network in this area, contractional structures trend parallel, rather than perpendicular, to regional maximum compressive stress directions predicted on the basis of geoid anomalies [*Sandwell et al.*, 1997]. A well-defined fabric of north-northeast trending wrinkle ridges dominates eastern Rusalka Planitia. To the west, Zaryanista Dorsa deformation belt wraps around a corona chain that contributed expansive lava flows to Rusalka Planitia [*Young and Hansen*, 2003].

[11] A subtle suite of northeast trending lineaments (likely fractures) pervades much of eastern Rusalka Planitia [*Young*, 2001]. These lineaments trend perpendicular to wrinkle ridges, mirroring the situation in Lavinia Planitia [*Squyres et al.*, 1992].

[12] Diana-Dali Chasmata is a zone of significant (for Venus) north-south extension, mantle diapirism, and volca-

nism. Lying south of the area shown in Figure 2, the chasmata marks Rusalka Planitia's southern boundary [Hansen and DeShon, 2002]. East of Diana-Dali Chasmata the trend of the zone of extension curves northward, cutting across Atla Regio, a broad topographic welt topped by several large volcanoes. An associated positive gravity anomaly implies that a mantle plume currently supports Atla Regio [Smrekar et al., 1997; Simons et al., 1997].

3. Data

[13] The NASA Magellan radar operated in two modes: (1) as a side-looking high-gain antenna for synthetic aperture radar (SAR) imagery and "spot" readings of radio emission and (2) as a nadir-looking low-resolution radar altimeter to acquire topographic and surface texture information. A single mapping cycle of S band (12.6-cm wavelength) SAR imagery with an effective resolution of ~ 100 m was collected over Poludnista Dorsa at an incidence angle of $\sim 40^\circ$ (illumination from the west). No stereo observations were acquired of Poludnista Dorsa; therefore any constraints on topography must come from radarclinometric analysis of single-illumination angle SAR images or through Magellan altimetry. Two cycles of west illuminated SAR imagery were obtained for Oya Dorsa, with incidence angles of 40° and 25° ; although the latter cycle had much poorer coverage, areas of overlap allow local stereo interpretation.

[14] Across Rusalka Planitia a single mapping cycle acquired altimetry data with 20-km gaps between north trending orbital tracks. Radar echoes received by the radar altimeter were separated into along-track Doppler-resolved cells or "footprints" [Ford and Pettengill, 1992]. The dimensions of each footprint are proportional to spacecraft altitude and velocity. At the latitude of Poludnista Dorsa (which corresponded to the periapsis of Magellan's orbit and thus the minimum range), footprints are ~ 8 km wide along track and ~ 12 km long across track. Spacecraft altitude (and thus radius once the spacecraft's orbit is determined) is derived by "fusing" all of the individual Doppler-separated pulses (to account for range changes due to spacecraft motion) received from a given location into a single range-sharpened echo. One of two techniques can be used to find the time delay and thus the range: fitting a model echo template to the data [Ford and Pettengill, 1992] or using simple threshold detection [Saunders et al., 1990]. The former is more precise, but it is more susceptible to topographic noise; the latter is typically more accurate in high-relief areas.

[15] Commonly, a gridded and interpolated form of the template-derived altimetry data (Global Topography Data Record (GTDR) [Ford and Pettengill, 1992; Rappaport et al., 1999]) is used to aid geologic mapping; however, this approach can introduce artifacts due to missing or anomalous footprints or interpolation. Of special concern are regions with abrupt transitions in radar properties. A common result is that the echo of footprints centered on relatively dull materials is dominated by the reflection from reflective material at the edge of the footprint. The result of the template fit is an off-nadir range and thus anomalously low topography. Because such transitions are typical for deformation belts, correction is necessary to constrain topography.

[16] Another source of error is topographic relief at higher spatial frequencies than the footprint resolution. This effect can result in sharp multiple echoes being received at the spacecraft, echoes that can bias the thresholding approach. The end result is that the template approach characterizes the "typical" topography of a footprint, whereas thresholding provides an approximate upper bound on elevation within a footprint. One way to deal with these problems is to automatically dispose of off-nominal footprints and to interpolate from the remaining data [Campbell et al., 1999; Rappaport et al., 1999]; however, given that analyzing topography at geologic contacts is a key part of this study, other methods are used here.

[17] The most obvious sign that an off-nadir reflection has been picked is the presence of the true nadir reflection earlier in the echo record; as such, the thresholding method will be less susceptible to off-nadir echoes. Failing that, direct examination of the power-time graph of the echo itself can reveal footprint quality.

[18] Data for each footprint are archived in altimetry and radiometry composite data records (ARCDR). Although a global gridded data set of threshold-derived topography has not been published (which allows for the correction of systematic orbital errors [Rappaport et al., 1999]), the threshold-derived radius and the echo time series for each footprint are included in the ARCDR data set. Directly mapping ARCDR-derived ALT footprints onto SAR images and geologic maps can help develop constraints on local topographic relationships; gridded topography and derived synthetic stereo products are useful for developing a regional context for geologic relationships.

4. Rusalka Planitia Deformation Belts

[19] Here we assess the context of some representative examples of broad, warped linear features, focusing on the interaction of these features with suites of regional tectonic structures. Vetsorgo Dorsum is representative of simple, wrinkle ridge-parallel warps within Rusalka Planitia; Oya Dorsa is a simple deformation belt that interacts with volcanic flow fields emerging from a nearby corona. Poludnista Dorsa, a complex deformation belt, will be analyzed in greater detail.

4.1. Vetsorgo Dorsum

[20] Vetsorgo Dorsum, which lies within southwestern Rusalka Planitia (162°E , 5°S), is an ~ 900 -km-long, 170-km-wide, nearly 900-km-high northwest trending warp (area 1 in Figure 2). Unlike the other belts discussed here, Vetsorgo Dorsum lacks evidence of pervasive deformation [DeShon et al., 2000]. Vetsorgo Dorsum is surrounded by moderately high backscatter flow material [Hansen and DeShon, 2002]; the core of Vetsorgo Dorsum comprises a kipuka of low-backscatter material cut by northeast trending fractures. Wrinkle ridges outline and parallel the warp. There is no obvious evidence of local volcanic sources associated with the warp.

[21] Vetsorgo Dorsum is the most pronounced of a series of gentle, parallel warps with wavelengths of ~ 200 – 300 km. Interactions with flow units indicate that uplift of these warps predated, at least in part, volcanism associated with the Diana Chasma system of coronae. The relevance of

these features to deformation belts is that although these broad linear warps lack a distinctive internal geologic signature, their overall topographic amplitude is similar at the 100-km scale to the other belts discussed herein. In addition, the warps integrate into a straightforward strain ellipse defined by the regional structures. These warps are similar to features identified in Venera SAR data as “broad arches” by *Frank and Head* [1990] and “class I ridge belts” by *Kryuchkov* [1990].

4.2. Oya Dorsa

[22] Oya Dorsa (155°E, 20°N) (area 2 in Figure 2) lies within eastern Llorona Planitia and forms the southernmost extension of the Vedma Dorsa system of deformation belts that extends to 58°N [*Raitala and Kauhanen*, 1991]. Oya Dorsa contains a 50-km-wide, 500-km-long pervasively deformed core, embedded within a broader, 1-km-high warp. The belt trends north-northeast; internal structures trend both parallel and perpendicular to the belt. Belt-parallel wrinkle ridges cut low-backscatter material in the adjacent lowland. However, 20 km outside the deformation belt, high-backscatter flow units sourced from Ituana Corona (153.5°E, 19.5°S) inundate the landscape. Wrinkle ridges curve into an eastward regional trend from the deformation belt.

[23] Extensional structures within Oya Dorsa trend both parallel and perpendicular to the main belt trend. A zone of low-lying material cut by orthogonal graben and flooded by undifferentiated material forms the northeast limit of Oya Dorsa. Despite evidence for later regional contraction these grabens have not been extensively reactivated. The channel (presumably volcanic in origin) Jutrzenka Vallis connects to one of these grabens. Flow direction through the channel is not clear; the possibility that Jutrzenka Vallis may reflect effusive volcanism tied to graben opening cannot be ruled out.

[24] Ituana Corona flow contacts contour around Oya Dorsa, and the flow surface slopes away from the belt, indicating that the main warp of Oya Dorsa continued to rise during and after the period of Ituana Corona activity [*Young and Hansen*, 2003]. Just south of the area in Figure 3b a 300-km flow field (Tie Fluctus) extends east of Oya Dorsa. Tie Fluctus is sourced from a channel that lies within a pass in Oya Dorsa, adjacent to the main Ituana Corona flow field. The pass stands higher than either the Ituana Corona flows or Tie Fluctus, implying either that (1) the warp of Oya Dorsa developed after much of the volcanic activity associated with Ituana Corona or (2) Oya Dorsa produced Tie Fluctus after warp development. Indeed, Oya Dorsa shows signs of late stage local volcanic activity; a 50-km-long channel emerges from a pit and tracks down the eastern slope of Oya Dorsa where it is buried by Ituana Corona-sourced flows.

5. Poludnista Dorsa

[25] Poludnista Dorsa (180°E, 12°N–3°S) is the most complex feature discussed here. It lies within eastern Rusalka Planitia (area 3 in Figure 2). The ~2000-km-long belt rises up to a kilometer high, with a structural core that ranges from nonexistent to 200 km across. Although overall the belt trends north, individual segments trend northwest

and north-northeast. The belt is divided into four segments, A–D, based on trend (Figure 3c).

5.1. Segment A

[26] Segment A (Figure 4), the highest segment, consists of a 100-km-wide, 425-km-long warp that reaches up to a kilometer above its surroundings. The main belt trends 315°, perpendicular to the regional topographic gradient. A broad topographic rise extends northeast of the main belt. Subtle periodic belt-parallel undulations occur southwest of the main belt, with the most prominent warp 250 km away from the main belt.

[27] Subtle belt-parallel ridges deform high-backscatter basal material. The ridges occur as gentle undulations a couple of kilometers across. Their relief is difficult to constrain without stereo imagery. However, given the local geometry of Magellan’s radar system, the lack of obvious radar shadowing of eastern limbs or overlay of the western limbs of the presumed folds requires that limb dips are <55°; therefore interlimb angles must exceed 70° (and are probably much greater). Limb dips are constrained to <25° (and an interlimb angle of 130°) on the basis of methodology of *McGill and Campbell* [2004], which uses the ratio of backscatter across the fold and assumes symmetry and planar limb surfaces.

[28] Domains, up to 20 km across, of high-backscatter material that lack evidence of deformation commonly separate the gentle folds. There is no evidence that these domains represent deposition that postdated fold formation; therefore we interpret that the spacing represents structural localization of folds. Fine-scale axis-parallel lineaments on some folds may represent parasitic folds.

[29] Sharply defined high-backscatter lineaments, typically paired with sharply defined low-backscatter lineaments, represent scarps and are interpreted as normal faults. The faults parallel the belt and commonly cut the belt-parallel ridges to the point of obscuring them. The scarps are closely spaced (<1 km) and continuous for up to 50 km along strike. This suite of structures is more prevalent on the northern side of the deformation belt where it extends out onto the topographic rise north of the main belt.

[30] No primary morphology is preserved in the high-backscatter material deformed by the gentle folds. Locally, patches of low-backscatter edifice material confined by the gentle ridges were emplaced following fold formation; there is no evidence that the edifice material was involved in folding. The high-backscatter basal material transitions into intermediate-backscatter material that lacks fine fold-parallel lineaments. These regions commonly contain edifices with summit craters that we interpret as evidence for local volcanism [e.g., *Guest et al.*, 1992]. Given the lack of high-resolution topographic data, it is difficult to assess the volume of extrusive material. Edifice materials both bury and are cut by the normal faults, indicating that belt-perpendicular extension and local magmatism overlapped spatially and temporally.

[31] A generally low backscatter surface of unknown origin and regional extent surrounds the high-backscatter belt material. Whether this surface corresponds to a single stratigraphic unit is difficult to determine with the current data. Contacts between this surface and the high-backscatter material are sharply defined and parallel local relief, sug-

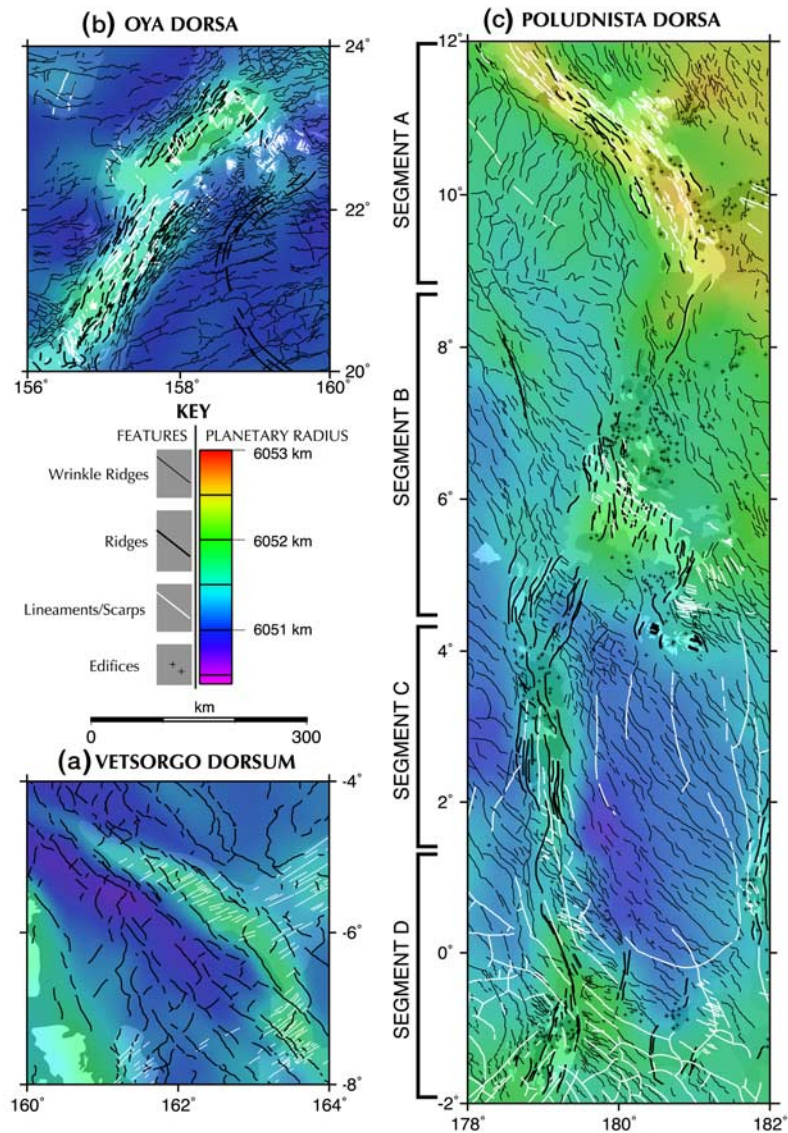


Figure 3. Mercator projection illustrating spatial correlation between topography and tectonic structures. (a) In Vetsorgo Dorsum (area 1 in Figure 2), coronae-sourced flows bury extensional lineaments, leaving those exposed on the warp visible. Sharply defined wrinkle ridges generally parallel the belt; no folds, as such, are visible. (b) Oya Dorsa (area 2 in Figure 2) contains belt-parallel folds and multiple sets of grabens and lineaments. Regionally, wrinkle ridges trend oblique to the belt but are closely spaced belt-parallel features on the flanks of Oya Dorsa. (c) Four major segments compose the main topographic extent of Poludnista Dorsa (area 3 in Figure 2). From north to south these are segment A, a southwest trending broad warp of moderately deformed material lying at ~ 6052.75 km; segment B, a transitional zone of slightly deformed volcanic flows and shields interacting with more deformed kipukas that trend south-southeast; segment C, a second warp that trends south and is dominated by patchy flows between narrow ridges lying at ~ 6051.10 km; and segment D, two parallel ridge-dominated kipukas with late shields within a broader network of crosscutting isotropic lineaments. Topography (gridded from altimetry and radiometry composite data records) is expressed as planetary radius. See text for details. Vetsorgo Dorsum relations are from *Hansen and DeShon* [2002].

gesting deposition of low-viscosity material on a rugged landscape. *Young and Hansen* [2003] describe this as undifferentiated flow material likely of volcanic origin. Undifferentiated flow material also truncates the scarps, indicating that activity on the faults predates flow emplacement.

[32] The contact between the high-backscatter belt material and undifferentiated flow material is sharp and embays

the fold topography of the belt material, implying that locally, the belt material is older. Flow material also embays volcanic shields. However, profiles constructed from individual radar altimeter tracks across segment A (Figure 5) show that undifferentiated flow material dips away from the structural core of the belt, indicating a local three-phase geological history: (1) emplacement, folding, and faulting

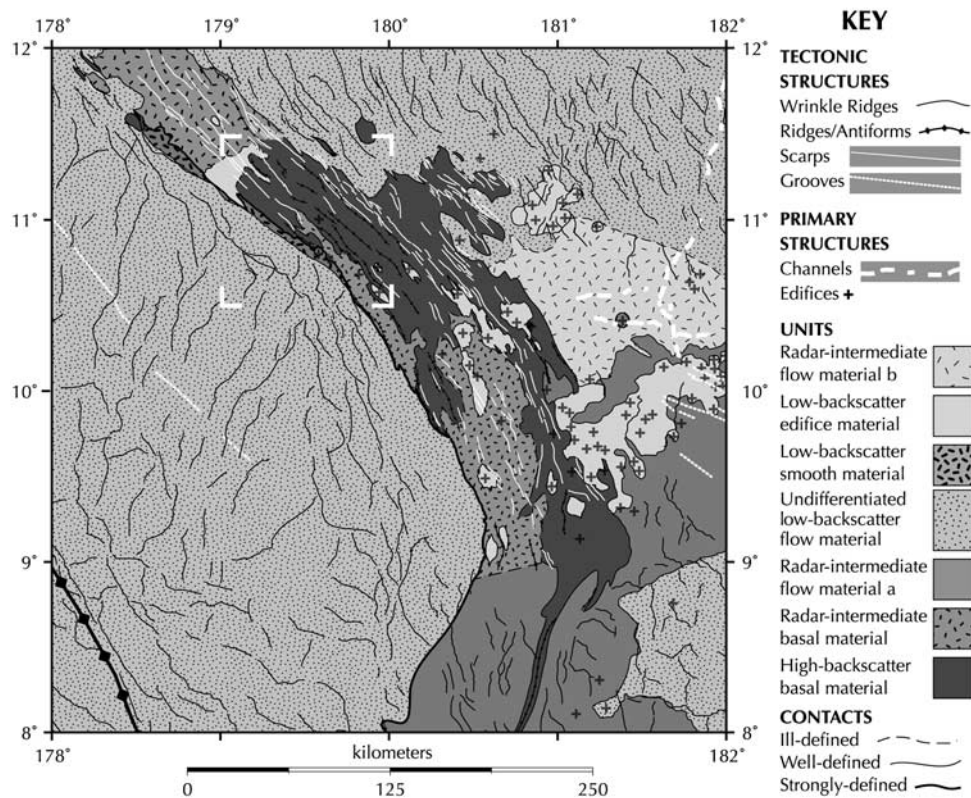


Figure 4. Geologic map of segment A of Poludnista Dorsa. White corners show the location of Figure 5.

of the high-backscatter belt material; (2) embayment of the belt by regionally expansive low-viscosity materials; and (3) larger-scale folding of the entire package of flow and belt material.

[33] Southwest of segment A, wrinkle ridges cut undifferentiated flow material. Between the main belt and the warp to the southwest, wrinkle ridges strike normal to the belt trend. Wrinkle ridges are uneven along trend and spaced $\sim 20\text{--}30$ km, with the exception of one well-developed wrinkle ridge that parallels the main belt along its southwestern slope. The boxy, narrow style of the wrinkle ridge distinguishes it from the older, within-belt folds. Northeast of the main belt several trends of crosscutting wrinkle ridges, spaced $\sim 5\text{--}10$ km, indicate a more subtle deformation history. A fan of fine lineaments and small shields extends eastward from the southeastern end of segment A.

[34] The volcanic patches in segment A become more expansive and coalesce toward the south until little of the high-backscatter material in segment A remains. A profusion of small (5–10 km across) shields, typically bearing summit pits, marks the northern section of segment B. Mottled low-backscatter and radar smooth low-relief materials, probably representing volcanic flows, surround the shields.

5.2. Segment B

[35] The ridges and scarps of segment B trend $\sim 20^\circ$ and extend ~ 500 km (Figure 6). The belt trends obliquely across the regional slope, complicating its topographic

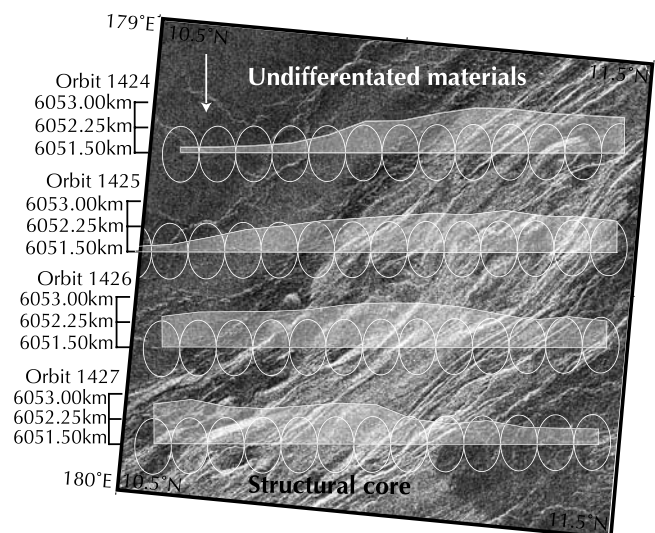


Figure 5. Synthetic aperture radar (SAR) image of a portion of segment A of Poludnista Dorsa. Radar illumination (white arrow) is from the west (top). Projected on top are the footprints from orbits 1424 to 1427 and profiles; vertical exaggeration is 7X. Note that the highest long-wavelength slopes are on the flanks of the structural core of the belt not in the core itself.

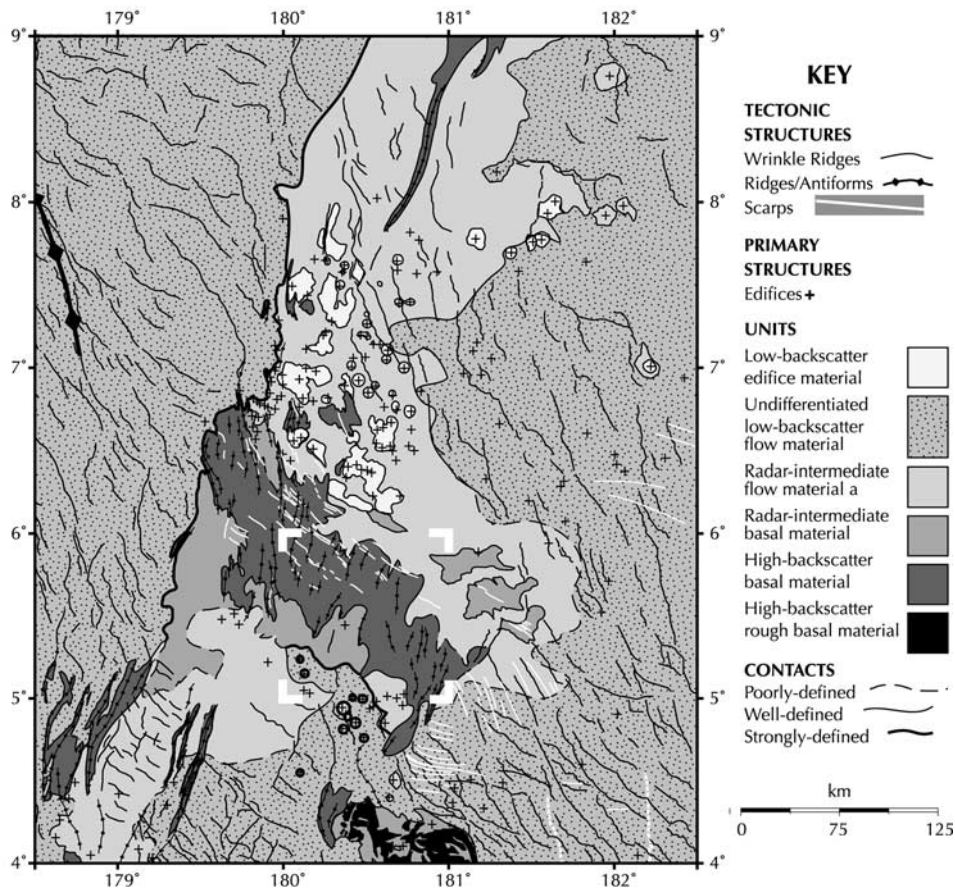


Figure 6. Geologic map of segment B of Poludnista Dorsa. White corners show the location of Figure 7.

expression. Volcanic edifices and flow units compose much of this segment and have a generally subdued relief of ~ 200 m above the surrounding terrain. A 150-km-long high-backscatter kipuka of gently deformed basal material cuts across the trend of segment B, rising up to 500 m above its surroundings (Figure 7). A north to north-northeast trending suite of gentle folds, with limb dips $< 13^\circ$ [after McGill and Campbell, 2004], defines the dominant structural trend within the kipuka. Much of the high-backscatter appearance of the kipuka material is due to pervasive fold-parallel lineaments. A subdued set of sharp northwest striking faults cut the folds. Outside of the high-backscatter kipuka but within the belt is a disorganized web of wrinkle ridges and a kilometer-scale reticulated network of lineaments that developed around some shields.

[36] In contrast, the contact between undifferentiated low-backscatter flow material and belt materials is well developed on the western edge of segment B and is compatible with older belt material. However, given that both the contact and the altimetry tracks trend north, it is difficult to determine the interaction between unit emplacement and topographic evolution.

[37] Southeast of the main belt, a second kipuka (Figure 6, 4°N , 181°E) composed of high-backscatter high-relief material embedded within intermediate-backscatter material lies within undifferentiated low-backscatter flow material.

North trending grabens (unmapped) within the high-backscatter high-relief material cut east trending folds; a subdued fold composed of high-backscatter material wraps around the western end of the belt, indicating a change in principal strain direction, either in space or in time.

[38] Well-developed wrinkle ridges that trend 325° , parallel to segment A but oblique to folds in segment B, cut undifferentiated flow material west of the belt. They do not cross the contact between undifferentiated material and belt material. To the east, wrinkle ridges are more weakly developed and are controlled in part by two crosscutting suites of closely spaced lineaments. These wrinkle ridges continue into the volcanic materials of the belt.

5.3. Segment C

[39] Segment C trends north, is ~ 500 km long, and has a maximum relief of 700 m (Figures 8 and 9). The segment is composed of low-backscatter edifice material, interpreted to represent low-relief volcanic constructs that embay narrow high-backscatter belt-parallel ridges. In plan view the ridges pinch and swell along trend with the highest points corresponding to the widest parts of the belt. Rare belt-parallel grooves cut the belt. A sharp contact between the edifice material and the surrounding lowland material is not apparent. Generating a reliable topographic profile is difficult in this region given the belt's north-south trend.

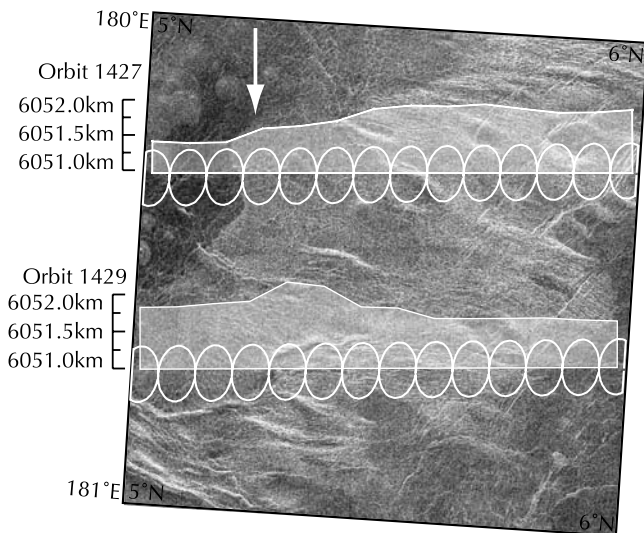


Figure 7. SAR image of a portion of segment B of Poludnista Dorsa. Radar illumination (white arrow) is from the west (top). Projected on top are the altimeter footprints from orbits 1424 to 1422 and profiles; vertical exaggeration is 14X. The main topographic slope is perpendicular to the trend of the folds and parallels the graben.

[40] A pair of north-northeast trending belt-bounding ridge complexes composed of high-backscatter material connects segments B and C. Wrinkle ridges between the ridges trend 300° , cutting mottled materials. The pair of ridges converge to the south and are buried by volcanic shields at 179°E , 4°N ; the ridge complexes emerge from beneath several generations of volcanic material at 179°E , 3°N , and diverge to form a maximum belt width of ~ 75 km at 179°E , 2.5°N , before converging at 179°E , 1.75°N . In all cases the high-backscatter material comprising the ridge complexes appears older than the surrounding material. Segment C ends at 179°E , 1.75°N , with belt-bounding ridges abruptly diverging 45° ; between the diverging sets of ridges, closely spaced, very straight lineaments that trend 305° cut undifferentiated flow material and are reactivated as nonsinusuous wrinkle ridges, analogous to the situation described by *DeShon et al.* [2000]. Sparse, belt-parallel grooves up to 400 km long cut all structures and materials.

[41] There are two forms of postridge material: 5-km-wide low-backscatter shields (the aforementioned edifice material), especially prominent at the northern convergence of the belt, and smooth radar intermediate flow material a, which has little evidence of primary structures, aside from embayment contacts with ridge materials. The shields, generally lacking summit pits, apparently overlie flow material a (Figure 8).

[42] West of the belt, gently curving northwest trending wrinkle ridges spaced ~ 30 km intersect rare belt-parallel wrinkle ridges; east of the belt, less well developed north-northwest trending wrinkle ridges are spaced ~ 10 km. Occasional wrinkle ridges to the east parallel the belt.

5.4. Segment D

[43] Segment D, the southernmost segment, has three components: a complex of ridges and shields that is a direct

continuation of segment C, a second, similar belt complex that lies 200 km to the east, and an ovoid structure that lies between the two belts (Figure 10). Segment D (west) is a continuation of the western ridge complex of segment C. The ridge complex changes from gentle ridges to the south to a single topographic east facing scarp with a relief of ~ 800 m and $\sim 300^\circ$ trend to the north. A single ridge visible in the altimetry data tops the ~ 200 -km-long scarp. A 20° trending belt of ridges and shields extends for ~ 150 km from the southern end of the topographic scarp.

[44] Estimating relief of the ridge complex is difficult because segment D lies on the southern slope of the eastern basin of Rusalka Planitia and trends near-parallel with the altimetry track; a best estimate is ~ 500 m. Segment D (east)

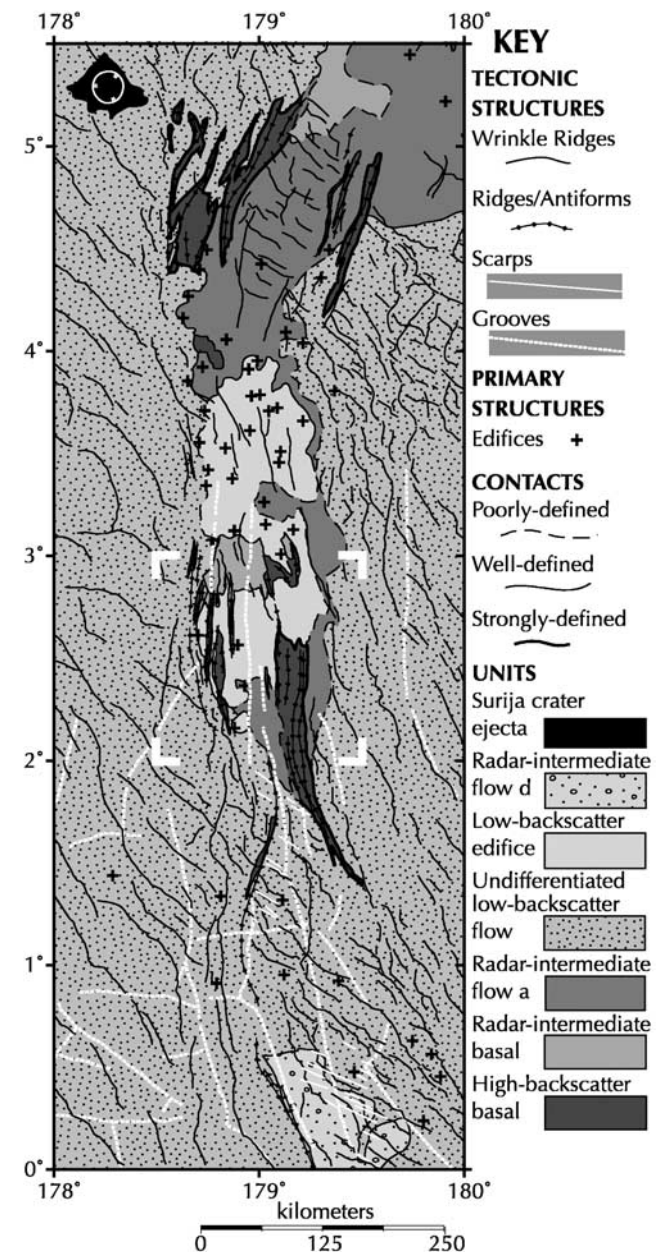


Figure 8. Geologic map of segment C of Poludnista Dorsa. White corners show the location of Figure 9.

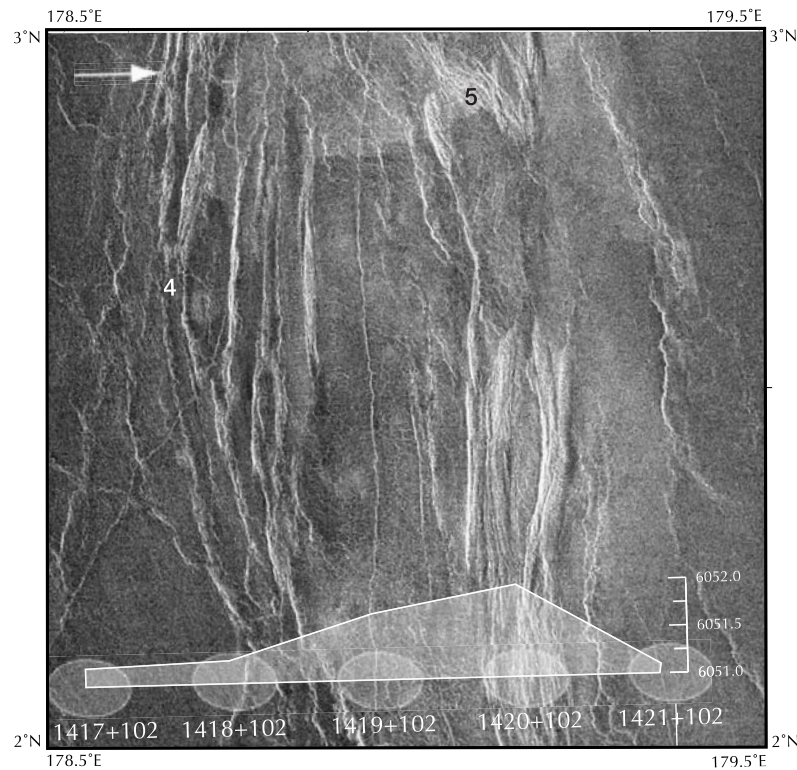


Figure 9. West illuminated (white arrow) SAR image of a portion of segment C of Poludnista Dorsa with projected radar altimeter footprints from orbits 1417 to 1421 and a derived profile with 14X vertical exaggeration. Two features indicate late stage volcanic activity: a shield with associated flows channeled between ridges (area 4) and truncation of structures by low-backscatter materials (area 5). Although volcanic flow material does not stand as high as the most prominent ridges, shields occur above the surroundings, indicating that deformation belt embayment occurs from within and does not result from passive flooding by outside sources.

is a belt of gentle ridges that approximately parallels the main belt of Poludnista Dorsa. This belt is ~ 400 km long with approximately 300- to 400-m relief. The ovoid has a subdued relief of ~ 200 m.

[45] Gentle belt-parallel folds, 2–3 km wide, composed of high-backscatter materials and bearing subtle trend-parallel lineaments enclose domains of radar intermediate flow material in both the western and eastern belts. Sharp, simple contacts may indicate either an embayed or thrust fault contact. The ovoid and the eastern belt are also embayed by material cut by a suite of closely spaced lineaments that trend 280° – 290° .

[46] High-backscatter material appears to emanate from the topographic scarp that composes the northern part of segment D (west). Whether this unit represents lava erupted from the scarp or a kipuka is difficult to determine. Subdued low-backscatter shield edifices ranging from 2 to 10 km wide overlie the folded high-backscatter materials; the surrounding undifferentiated low-backscatter flow material, in turn, locally overlies the shields.

[47] Well-developed northwest trending wrinkle ridges cut all units except the high-backscatter material. Also cutting all units is an extensive, pseudoisotropic network of curvilinear grooves [Hansen and DeShon, 2002]. Grooves cross one another or are truncated in Y- or (more

commonly) T-type intersections. Typical groove spacing is ~ 20 km. Some grooves transition into curvilinear ridges along strike, which, in turn, are connected to wrinkle ridges. The inference is that the grooves predate wrinkle ridge formation and are reactivated. Further discussion of these grooves is beyond the scope of this paper.

6. Synthesis

6.1. Internal Structure

[48] The absence of primary structures and the presence of fine lineaments on a 250-m length scale on the basal high-backscatter material argue for pervasive deformation of the locally earliest material in the belt's structural core. However, the comparatively gentle geometry of the folds that deform the "basal" high-backscatter material along with minimal evidence for brittle failure indicates that the amount of finite contractional strain is low. The short structural wavelength of the folds indicates a thin (on the order of 1 km) mechanical layer at the time of fold formation. A locally early extensional fabric, composed of normal faults, fractures, and grabens with trends $310^\circ \pm 5^\circ$, occurs in at least three segments of Poludnista Dorsa, irrespective of belt orientation. Extension occurs high on the main warp of the belt, to the side of the main warp, and

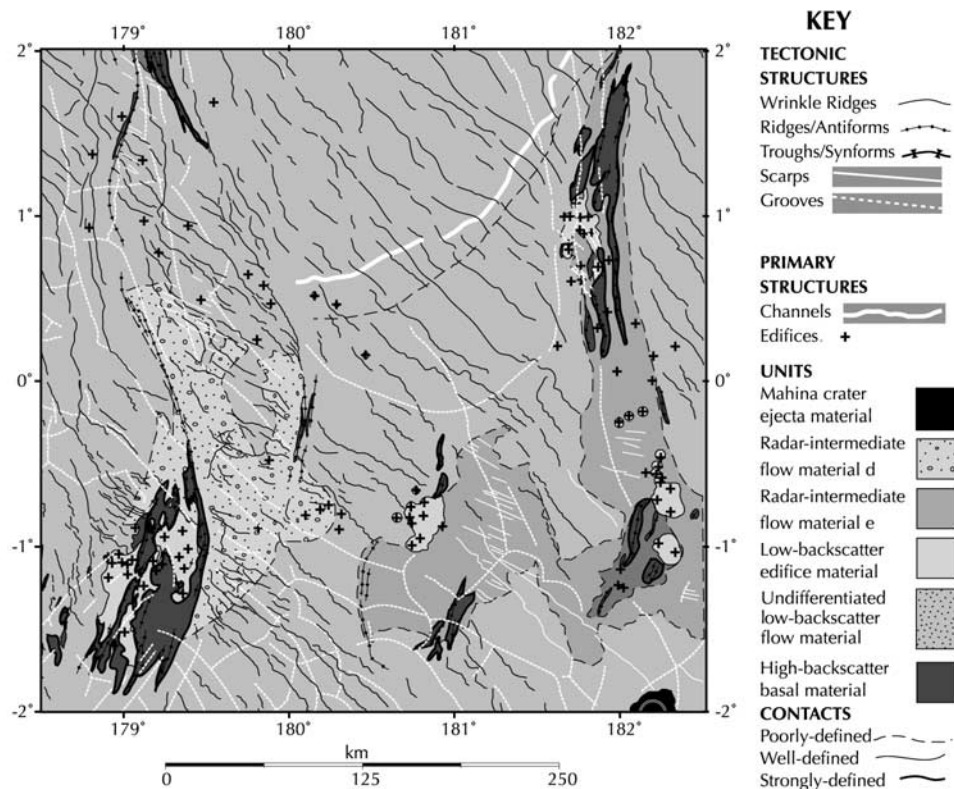


Figure 10. Geologic map of segment D of Poludnista Dorsa.

across the trend of the main warp topography. On Oya Dorsa some well-developed extensional structures lie well off the belt.

[49] Some workers [e.g., *Solomon and Head, 1991; Phillips and Hansen, 1994*] have suggested slope failure as a mechanism for generating fractures in deformation belts; however, in Poludnista Dorsa, slopes and extensional structures lack spatial correlation, and parallel alignment between the strike of the local steepest slope and graben occurs only at segment A. Slope failure would require that the topography of the deformation belt has been modified since extension occurred. The suggestion that flexural bending of the lithosphere might cause extensional faulting [*Banerdt et al., 1997*] is also inconsistent with spatial relations. There is no consistent orientation between warp hinge line and normal faults. Although both of these mechanisms may have contributed to the total strain resolved on these structures, neither seems to provide a simple explanation for their formation. An additional important point is that broad warps of similar relief lack evidence of slope failure. Without speculating on the specific origin of this fabric, scarp distribution and orientation within Poludnista Dorsa and Oya Dorsa imply that extension cannot be solely tied to longer wavelengths of belt topography.

[50] Could extension be related to the reactivation of structures that predate folding within the belt? There is little evidence for linear, sharply bound contractional features in the belt cores that might indicate contractional reactivation of the graben; grabens do not cut the surrounding undifferentiated flows material. Outside of the

core of Poludnista Dorsa, however, fine lineaments trending $\sim 310^\circ$ intersect wrinkle ridges and locally develop positive topography, suggesting reactivation of an existing low-strain fracture set.

6.2. Tectonic Environment

[51] Radar altimeter footprint profiles confirm that surfaces surrounding the outcrop of the deformation belt core tend to dip away up from the belt axis with slopes of up to a couple of degrees (see Figures 5, 7, and 9). These slopes define the long-wavelength topography of the belt. In most cases, materials locally younger than the belt materials underlie the surrounding surfaces (as indicated by embayment relationships with folds). If the volcanic material had a source external to the deformation belt and tended toward an equipotential deposition surface, then the tilting of these surfaces would be one of the last phases of geologic evolution recorded at the belts. In most cases, there is no evidence for an abrupt slope break related to the belt core, even though the method used to define topography would tend to enhance elevations in the comparatively rough terrain associated with the radar bright materials.

[52] For segment A most of the long-wavelength deformation can be explained by surface warping after local deposition of the surrounding undifferentiated materials. There is no evidence that formation of the short-wavelength gentle folds was synchronous with development of the broad long-wavelength topographic warp, although the preservation of high-backscatter material indicates that some local relief predated emplacement of undifferentiated flow material.

[53] Similar relationships have been reported for other deformation belts on Venus. The topographic warp of Oya Dorsa in Llorona Planitia shows clear time transgressive behavior with respect to adjacent corona flow fields [Young and Hansen, 2003], Stewart and Head [2000] document time transgressive interactions between Vedma Dorsa and local volcanic channels in Ganiki Planitia, and profiles using GTDR at Pandrosos Dorsa [Rosenberg and McGill, 2002; McGill, 2003] also indicate a spatial offset between topography and surface contacts, hinting at similar temporal decoupling of different spatial length scales.

[54] The inferred contact between the structural core of the belt and the surrounding material tends to be best expressed on the western, “downslope” side of the belt. This may reflect structural vergence, or it may be due to contrasting styles of flow emplacement, with a regional depocenter to the west and more localized eruptive centers related to Atla Regio to the east. Regional wrinkle ridges postdate much of deformation belt evolution. Although reactivation should always be considered possible with wrinkle ridges, the interpretation that wrinkle ridges represent late stage deformation is supported by the observations that (1) belt-parallel wrinkle ridges only seem to form on the slope of the warp, (2) wrinkle ridges that trend oblique to the belt tend to curve into parallelism with the belt, and (3) wrinkle ridges that cut the belt tend to reactivate belt structures. Wrinkle ridges never cut the lineated high-backscatter deformed material, a relationship that may result from the material’s mechanical structure (as indicated by the fine lineaments) and/or layering relative to wrinkle ridge orientation.

[55] Early work relating short-wavelength deformation to longer-wavelength warping presumed a weak lower crust of regional extent due to high surface temperature [Zuber, 1987b, 1990]. If a lithosphere with such a layering is remotely stressed, two periodic wavelengths of deformation reflecting the thicknesses and strengths of the two important mechanical layers (the upper crust and the upper mantle) are predicted to emerge simultaneously.

[56] Geologic constraints found here suggest either that strong mechanical layering of the lithosphere was temporally constrained to the core of the belt or that a pervasive weak lower crustal layer was restricted to an early period of the belt’s evolution. Although a broad warp may have formed in the early part of the belt’s history, such formation is not required by the data. Thus flexure of a strong upper mantle layer is not required for the deformation patterns in the core of the fold belt.

[57] Where folds of the belt core meet undifferentiated flow material deformed by the long-wavelength warp, the short-wavelength folds are older. We cannot directly extend this evidence into the belt core, but there, too, when compared to extension and local volcanic activity, short-wavelength folds appear to be locally oldest. These observations are compatible either with thickening of a single regional mechanical layer with time or with a locally thin layer corresponding to the belt core responding to regional stresses differently from the surrounding thicker lithosphere. Local volcanic activity argues for local high heat flow and crustal dilation and thus favors the latter hypothesis; additional evidence for strain localization is discussed in more detail in section 7.

6.3. Volcanism

[58] Locally sourced late stage volcanic flows and shields are prevalent along the deformation belt. The lack of substantial caldera development may imply that rates of magmatism are too low to allow subsurface magma chamber development; alternatively, rising magma may have been less dense than the crust because of melt composition and/or temperature and thus did not pond at a “neutral buoyancy” level [cf. Head and Wilson, 1992]. This observation of deformation belt volcanism reinforces the evidence for substantial volcanic activity that has also been described in post-Magellan mapping of the deformation belts of Vinmara Planitia [Addington, 2001; Rosenberg and McGill, 2002; McGill, 2003]. “Mottled plains” material described in Lavinia Planitia belts likely represents shield volcanism [Squyres et al., 1992]. The channel on Oya Dorsa indicates that low-viscosity melt generation accompanies long-wavelength warp formation.

[59] The apparent paradox of local volcanic activity against a background of contractional strain might be explained by four end-member mechanisms: (1) shallow level anatexis due to overthickening of the crust, (2) tectonic dilation perpendicular to shortening providing space for melt to rise, (3) reversal in the local stress state, or (4) massive subcrustal melting that generates enough magma to break through a lithosphere in compression. The lack of caldera or pits in most parts of the belt limits the possibility of large melt bodies at shallow levels in the crust [e.g., Crumpler et al., 1997], although pervasive, in situ “sweating” of the upper crust remains a possibility [Hansen and Bleamaster, 2002]. Melts originating in the mantle would have implications for the stress state of the lithosphere. Solomon et al. [1992] suggested that melt could reach the surface through fractures due to extensional bending at the top of the broad warp. However, this hypothesis predicts compression on the underside of the bending layer, which should inhibit the emergence of melt from the mantle. It is difficult to generate simultaneous orthogonal tensional and compressional failure throughout the lithosphere by Anderson’s criteria without high pore fluid pressures [Squyres et al., 1992], radial stress fields [Ghent and Hansen, 1999], or noncoaxial shear. The dehydrated state of Venus’s atmosphere argues against the first possibility (although the full implications of supercritical CO₂ in Venus’s lower atmosphere have not been fully explored), and the strain recorded within Poludnista Dorsa is not compatible with the latter two mechanisms (there is evidence for noncoaxial strain in Lavinia Planitia [Squyres et al., 1992; Koenig and Aydin, 1998]). The implication is that it is difficult to kinematically generate the space required for eruption while folding is occurring, although the reactivation of early structures may provide an avenue for effusion.

[60] The transition from folding to volcanism and the related observation that in the northern part of the belt that extension and local volcanism appear to overlap in time indicate that recorded strain and volcanic activity may reflect a local temporal transition from belt orthogonal shortening to limited extension. Given that there is also evidence of late long-wavelength warping, the following tectonic sequence may explain volcanism: (1) local thin skin contraction, (2) extension and related pressure release melting and volcanic activity, and (3) a transition to thick

skin contraction. As we have little evidence as to the compositions of the volcanic materials and cannot assess whether they represent pressure release melting of the mantle, testing this hypothesis is difficult; however, the existence of the late channel on Oya Dorsa indicates that pressure release melting may not be a complete explanation for deformation belt volcanism.

6.4. Stratigraphy

[61] The local stratigraphic column found in many of the described regions superficially resembles those found at different locations on Venus by other workers [*Basilevsky et al.*, 1997; *Basilevsky and Head*, 2000; *Ivanov and Head*, 2001]. These workers have suggested that these repeated successions represent direct evidence for globally synchronous phases of singular geological style. However, Venus lacks an independent time index that can spatially resolve local geological units, making it difficult to test the claim of global stratigraphy [*Campbell*, 1999]. Indeed, the observed succession of high-relief units preceding younger low-relief units may simply be the product of local preservational bias associated with burial rather than reflecting global or regional correlations in tectonic style. Given the uncertainties inherent in geological correlations without independent temporal indexes [*Hansen*, 2000], we choose not to pursue the implications for global geological history further in this paper.

7. Discussion

[62] Working hypotheses for the formation of Poludnista Dorsa must (1) account for the polyharmonic and pervasive deformation of the locally oldest material, (2) allow for local volcanic activity, (3) address abrupt transitions in along-strike geology, (4) address the late development of the topographic warp, and (5) accommodate the range of orientations and locations (relative to the axis of contraction) of extension, including completely off the belt. Models must also account for broad warps both with and without exposed belts of deformed material found within Rusalka Planitia. These features have similar long-wavelength amplitudes but differ in orientation. Specifically, the warps tend to parallel the trend of the regional wrinkle ridge fabric, whereas deformation belts are discordant with regional wrinkle ridge trends. Locally, individual wrinkle ridge trends swing into parallelism with deformation belts, apparently in response to broad topography. These relationships indicate that warp formation likely predated, or overlapped with, local wrinkle ridge development. Given that regional wrinkle ridge trends can be explained by shortening due to the swell-push force imposed by regional geoid anomalies [*Sandwell et al.*, 1997], it is tempting to explain warp orientation by a similar mechanism. However, this model cannot directly explain the orientation of deformation belts in the Rusalka Planitia region.

[63] It is possible that similar swell-push stresses, guided locally by mechanical heterogeneities, drove warp development. This hypothesis would imply that the exposed deformation belt core represents a spatially localized heterogeneity, and as such, it would not be rheologically representative of the material that underlies undifferentiated flow material in the lowlands.

[64] A second argument for the localized nature of deformation in Poludnista Dorsa is the along-trend localization in geologic style and orientation. Amounts of volcanic activity vary considerably along the belt, as does topography. Fold trends in the structural core along the length of the belt vary by $>50^\circ$. All of these features imply significant local influence on belt evolution.

[65] It has been suggested that the proximal cause of many deformation belts is regional strike-perpendicular compression [e.g., *Zuber*, 1987b, 1990; *Banerdt et al.*, 1997], probably driven by coupling of the convecting mantle with the lithosphere given the lack of a low-viscosity zone in Venus's mantle [*Phillips*, 1990] (Figure 11). The primary evidence for this hypothesis is the structural wavelengths over hundreds of kilometers in Vinmara Planitia [*Zuber*, 1987b, 1990] and Lavinia Planitia [*Solomon et al.*, 1992] and the 100-km-scale "ridge-like warp" profile [*Banerdt et al.*, 1997]. Shorter-wavelength structures within some deformation belts were interpreted to be the result of decoupling of the upper crust from the lower lithosphere due to high surface temperatures [*Zuber*, 1987b]. However, as noted in section 1, the results of *Mackwell et al.* [1998] indicate that an anhydrous lower crust is much stronger than previously thought and would not easily allow decoupling.

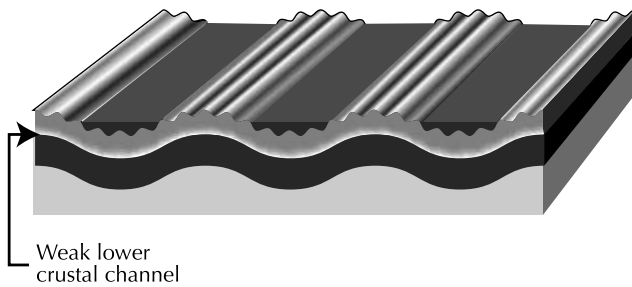
[66] Deuterium isotope chemistry is consistent with the interpretation that Venus's atmosphere may have had much higher water content in the last billion years [*Donahue*, 1999]. If Venus's crust was wetter in the past, crustal decoupling may have occurred, and thus multiple structural wavelengths could be symptomatic of ancient deformation (Figure 11). The history of water on Venus remains controversial [*Donahue et al.*, 1997], and the timing of deformation belt formation relative to Venus's surface history remains unconstrained.

[67] Although regional contraction may provide an explanation for unornamented lowland warps, this mechanism in its simplest form has difficulty accounting for the more complex geologic histories of deformation belts. *Frank and Head* [1990], working from 1- to 2-km resolution Venera SAR data, suggested that there was an evolutionary sequence from simple warps through more complex deformation belts to zones of full-fledged underthrusting. Our study does not support this hypothesis. While broad warps and deformation belts appear to be analogous features, reflecting regional shortening, they differ in that the latter is localized by lithospheric heterogeneity exposed in the structural core of the belt.

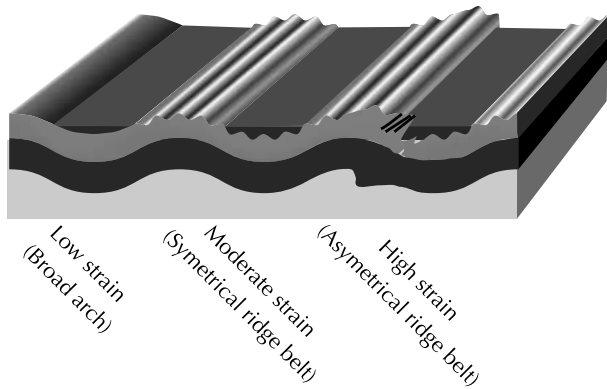
[68] *Squyres et al.* [1992] suggest that vigorous mantle convection could induce crustal thickening over a local downwelling. Elements unaddressed by this model include how the mantle convection cell is anchored to the emerging belt and how melt is generated.

[69] A candidate process for driving deformation belt evolution could be delamination of the lithospheric mantle [e.g., *Bird*, 1979; *Phillips and Hansen*, 1994] (Figure 12). A portion of the lithosphere is destabilized, either through sublithospheric convection or as a Rayleigh-Taylor instability, and gravitationally descends, peeling away from the crust as a sublinear mass. Warm mantle moves up the sides of the descending material, causing contraction above the locus of downwelling and extension and thinning above the margins of the downwelling. Once delamination is com-

Regional, dual wavelength model [Zuber 1990]



Evolutionary model [Frank & Head 1990]



Lithospheric inheritance model [this paper]

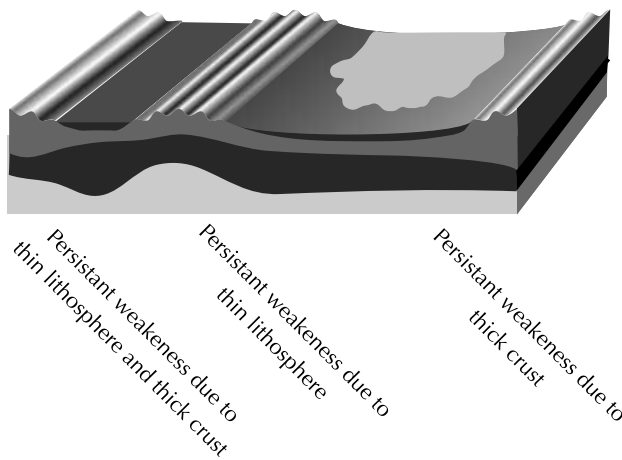


Figure 11. Simplified cylindrical cartoons of possible models for deformation belt formation. Zuber [1990] suggested that the regional harmonic buckling of a mechanically layered lithosphere, with long-wavelength troughs buried by volcanic materials, could explain the appearance of belts of Vinmara Planitia. Frank and Head [1990] suggested that broad warps may represent an early phase of deformation belt formation. The model of belt evolution favored in this study is that belts represent persistent lithospheric heterogeneities. The heterogeneities could be manifested as variations in crustal thickness or lithospheric thickness.

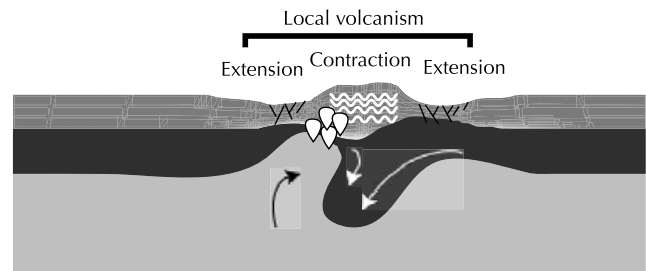
plete, the deformation belt would have a thinned lithosphere and enhanced volcanism and would be tectonically weakened. A lithospheric heterogeneity could persist if increased magmatism and local convergence thicken the crust. If the delaminating lithosphere peels off in a particular direction, the loci of contractional and extensional deformation could overlap over time and perhaps account for the complexity discussed herein. Delamination could provide for local early contraction of a thin mechanical layer; local high heat flow and volcanism; structural vergence of long, narrow, regional-scale linear features; and a residual localized heterogeneity in the lithosphere. Delamination has also been proposed to play a key role in coronae formation [Smrekar and Stofan, 1997]. The deformation annuli of many coronae have similar widths to deformation belts. However, delamination requires the presence of a low-viscosity layer between the crust and lithosphere (in Smrekar and Stofan's [1997] model an impinging thermal mantle plume provides this layer), apparently at odds with our current understanding of Venus's rheology [Mackwell et al., 1998].

8. Conclusions

[70] This study of Poludnista Dorsa demonstrates that deformation belts record complex time transgressive evolu-

Phase 1: Local deformation

(Delamination? [Phillips & Hansen 1994])



Phase 2: Regional shortening

(Convective coupling? [Phillips 1990; Squyres et al 1992]; swell push force? [Sandwell et al 1997])

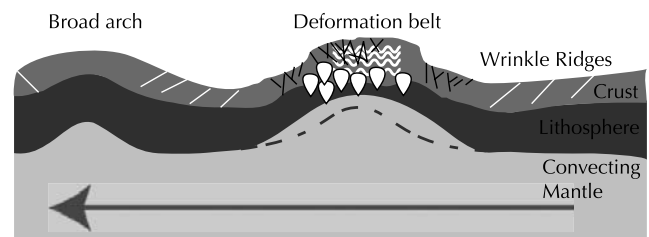


Figure 12. Cartoon of a generic delamination model. In phase 1, foundering of the thermal lithosphere causes local contraction and marginal extension. As the lithosphere peels away, pressure release melting of rising hot mantle causes crustal thickening and local volcanism. In phase 2, later regional contraction causes isolated buckling focused on weak deformation belts and harmonic buckling (broad warps) at long wavelengths. Early short-wavelength grabens are locked into a thickening mechanical layer and are preferentially obscured by subsequent resurfacing; later adjacent wrinkle ridges may reflect reactivation of these features.

tion. Both contractional structures and volcanism are key elements of deformation belt geology, and these potentially conflicting processes must be reconciled in any model of formation. While common geologic elements persist along the trend of the belt, many details differ, and strong local segmentation occurs. Geologic relations reported herein do not require synchronous development of short and long structural wavelengths; furthermore, it is likely that the short-wavelength structures in the structural core of the belt represent a local tectonic regime and the long-wavelength warp formed in response to later regional processes. Delamination may represent an alternative or an addendum to regional contraction as the process responsible for belt formation.

[71] **Acknowledgments.** The authors thank M. Kreslavsky and an anonymous reviewer for helpful comments. We thank N. Lang, B. Campbell, and G. McGill for additional useful discussions. This work was supported by NASA grants NAG5-4562 and NAG5-9142 to Hansen and to Southern Methodist University and University of Minnesota at Duluth, respectively. The McKnight Foundation provided additional support.

References

- Addington, E. A. (2001), A stratigraphic study of small volcano clusters on Venus, *Icarus*, *149*(1), 16–36, doi:10.1006/icar.2000.6529.
- Balme, M. R., P. R. Sammonds, C. Vita-Finzi, and J. P. Couchman (2004), Experimental and theoretical fracture mechanics applied to fracture of the crust of Venus, *J. Geophys. Res.*, *109*, E03005, doi:10.1029/2002JE001992.
- Banerdt, W. B., and C. G. Sammis (1992), Small-scale fracture patterns on the volcanic plains of Venus, *J. Geophys. Res.*, *97*(E10), 16,149–16,182.
- Banerdt, W. B., G. E. McGill, and M. T. Zuber (1997), Plains tectonics on Venus, in *Venus II: Geology, Geophysics, Atmosphere, and Solar Wind Environment*, edited by S. W. Bougher, D. M. Hunten, and R. J. Phillips, pp. 901–930, Univ. of Ariz. Press, Tucson.
- Basilevsky, A. T., and J. W. Head (1988), The geology of Venus, *Annu. Rev. Earth Planet. Sci.*, *16*, 295–317.
- Basilevsky, A. T., and J. W. Head (2000), Geological units on Venus: Evidence for their global correlation, *Planet. Space Sci.*, *48*, 75–111.
- Basilevsky, A. T., J. W. Head, G. G. Schaber, and R. G. Strom (1997), The resurfacing history of Venus, in *Venus II: Geology, Geophysics, Atmosphere, and Solar Wind Environment*, edited by S. W. Bougher, D. M. Hunten, and R. J. Phillips, pp. 1047–1086, Univ. of Ariz. Press, Tucson.
- Bilotti, F., and J. Suppe (1999), The global distribution of wrinkle ridges on Venus, *Icarus*, *139*(1), 137–157, doi:10.1006/icar.1999.6092.
- Bird, P. (1979), Continental delamination and the Colorado Plateau, *J. Geophys. Res.*, *84*(B13), 7561–7571.
- Campbell, B. A. (1999), Surface formation rates and impact crater densities on Venus, *J. Geophys. Res.*, *104*(E9), 21,951–21,955.
- Campbell, B. A., D. B. Campbell, and C. H. DeVries (1999), Surface processes in the Venus highlands: Results from analysis of Magellan and Arecibo data, *J. Geophys. Res.*, *104*(E1), 1897–1916.
- Crumpler, L. S., J. C. Aubele, D. A. Senske, S. T. Keddie, K. P. Magee, and J. W. Head III (1997), Volcanoes and centers of volcanism on Venus, in *Venus II: Geology, Geophysics, Atmosphere, and Solar Wind Environment*, edited by S. W. Bougher, D. M. Hunten, and R. J. Phillips, pp. 697–756, Univ. of Ariz. Press, Tucson.
- DeShon, H. R., D. A. Young, and V. L. Hansen (2000), Geologic evolution of southern Rusalka Planitia, Venus, *J. Geophys. Res.*, *105*(E3), 6983–6995.
- Donahue, T. M. (1999), New analysis of hydrogen and deuterium escape from Venus, *Icarus*, *141*(2), 226–235, doi:10.1006/icar.1999.6186.
- Donahue, T. M., D. H. Grinspoon, R. E. Hartle, and R. R. Hodges Jr. (1997), Ion/neutral escape of hydrogen and deuterium: Evolution of water, in *Venus II: Geology, Geophysics, Atmosphere, and Solar Wind Environment*, edited by S. W. Bougher, D. M. Hunten, and R. J. Phillips, pp. 385–414, Univ. of Ariz. Press, Tucson.
- Ford, P. G., and G. H. Pettengill (1992), Venus topography and kilometer-scale slopes, *J. Geophys. Res.*, *97*(E8), 13,103–13,114.
- Frank, S. L., and J. W. Head (1990), Ridge belts on Venus: morphology and origin, *Earth Moon Planets*, *50–51*, 421–470.
- Ghent, R., and V. Hansen (1999), Structural and kinematic analysis of eastern Ovda Regio and Venus: Implications for crustal plateau formation, *Icarus*, *139*(1), 116–136.
- Grosfils, E. B., and J. W. Head (1994), The global distribution of giant radiating dike swarms on Venus: Implications for the global stress state, *Geophys. Res. Lett.*, *21*(8), 701–704.
- Guest, J. E., M. H. Bulmer, J. Aubele, K. Beratan, R. Greeley, J. W. Head, G. Michaels, C. Weitz, and C. Wiles (1992), Small volcanic edifices and volcanism in the plains of Venus, *J. Geophys. Res.*, *97*(E10), 15,949–15,966.
- Hansen, V. L. (2000), Geologic mapping of tectonic planets, *Earth Planet. Sci. Lett.*, *176*(3–4), 527–542.
- Hansen, V. L., and L. F. Bleamaster III (2002), Distributed point source volcanism: A mechanism for regional plains resurfacing, Venus, *Lunar Planet. Sci. Conf.*, *XXXIII*, Abstract 1061.
- Hansen, V. L., and H. R. DeShon (2002), Geologic map of the Diana Chasma quadrangle (V-37), *U.S. Geol. Surv. Geol. Invest. Ser.*, *I-2752*.
- Head, J. W., and L. Wilson (1992), Magma reservoirs and neutral buoyancy zones on Venus: Implications for the formation and evolution of volcanic landforms, *J. Geophys. Res.*, *97*(3), 3877–3903.
- Ivanov, M. A., and J. W. Head (2001), Geology of Venus: Mapping of a global geotraverse at 30°N latitude, *J. Geophys. Res.*, *106*(E8), 17,515–17,566.
- Ivanov, M. A., and J. W. Head (2002), Geologic map of the Lavinia Planitia quadrangle (V-55), Venus, *U.S. Geol. Surv. Geol. Invest. Ser.*, *I-2783*.
- Koenig, E., and A. Aydin (1998), Evidence for large-scale strike-slip faulting on Venus, *Geology*, *26*(6), 551–554.
- Kryuchkov, V. P. (1990), Ridge belts; are they compressional or extensional structures?, *Earth Moon Planets*, *50–51*, 471–491.
- Lawrence, K. P., and R. J. Phillips (2003), Gravity/topography admittance inversion on Venus using niching genetic algorithms, *Geophys. Res. Lett.*, *30*(19), 1994, doi:10.1029/2003GL017515.
- Mackwell, S. J., M. E. Zimmerman, and D. L. Kohlstedt (1998), High-temperature deformation of dry diabase with application to tectonics on Venus, *J. Geophys. Res.*, *103*(B1), 975–984.
- McGill, G. E. (1993), Wrinkle ridges, stress domains, and kinematics of Venusian plains, *Geophys. Res. Lett.*, *20*(21), 2407–2410.
- McGill, G. E. (2003), Kinematics of a linear deformation belt; the evolution of Pandrosos Dorsa, Venus, *Lunar Planet. Sci. Conf.*, *XXXIV*, Abstract 1012.
- McGill, G. E., and B. A. Campbell (2004), Ages of Venusian ridge belts relative to regional plains, *Lunar Planet. Sci.*, *XXXV*, Abstract 1143.
- Phillips, R. J. (1990), Convection-driven tectonics on Venus, *J. Geophys. Res.*, *95*(B2), 1301–1316.
- Phillips, R. J., and V. L. Hansen (1994), Tectonic and magmatic evolution of Venus, *Annu. Rev. Earth Planet. Sci.*, *22*, 597–654.
- Phillips, R. J., C. L. Johnson, S. L. Mackwell, P. Morgan, D. T. Sandwell, and M. T. Zuber (1997), Lithospheric mechanics and dynamics of Venus, in *Venus II: Geology, Geophysics, Atmosphere, and Solar Wind Environment*, edited by S. W. Bougher, D. M. Hunten, and R. J. Phillips, pp. 1163–1204, Univ. of Ariz. Press, Tucson.
- Raitala, J., and K. Kauhanen (1991), Ridge belt tectonics of Ganiki Planitia on Venus, *Earth Moon Planets*, *53*(2), 127–148.
- Rappaport, N. J., A. S. Konopliv, A. B. Kucinskias, and P. G. Ford (1999), An improved 360 degree and order model of Venus topography, *Icarus*, *139*(1), 19–31, doi:10.1006/icar.1999.6081.
- Rosenberg, E., and G. McGill (2002), Geological map of the Pandrosos quadrangle (V-5), Venus, *U.S. Geol. Surv. Geol. Invest. Ser.*, *I-2721*.
- Sandwell, D. T., C. L. Johnson, F. Bilotti, and J. Suppe (1997), Driving forces for limited tectonics on Venus, *Icarus*, *129*(1), 232–244, doi:10.1006/icar.1997.5721.
- Saunders, R. S., G. H. Pettengill, R. E. Arvidson, W. L. Sjogren, W. T. K. Johnson, and L. Pieri (1990), The Magellan Venus radar mapping mission, *J. Geophys. Res.*, *95*(B6), 8339–8355.
- Simons, M., S. C. Solomon, and B. H. Hager (1997), Localization of gravity and topography; constraints on the tectonics and mantle dynamics of Venus, *Geophys. J. Int.*, *131*(1), 24–44.
- Smrekar, S. E., and E. R. Stofan (1997), Corona formation and heat loss on Venus by coupled upwelling and delamination, *Science*, *277*(5330), 1289–1294.
- Smrekar, S. E., W. S. Kiefer, and E. R. Stofan (1997), Large volcanic rises on Venus, in *Venus II: Geology, Geophysics, Atmosphere, and Solar Wind Environment*, edited by S. W. Bougher, D. M. Hunten, and R. J. Phillips, pp. 845–878, Univ. of Ariz. Press, Tucson.
- Solomon, S. C., and J. W. Head (1991), Fundamental issues in the geology and geophysics of Venus, *Science*, *252*(5003), 252–260.
- Solomon, S. C., et al. (1992), Venus tectonics: An overview of Magellan observations, *J. Geophys. Res.*, *97*(E8), 13,199–13,255.
- Squyres, S. W., D. G. Jankowski, M. Simons, S. C. Solomon, B. H. Hager, and G. E. McGill (1992), Plains tectonism on Venus: The deformation belts of Lavinia Planitia, *J. Geophys. Res.*, *97*(E8), 13,579–13,599.

- Stewart, E. M., and J. W. Head (2000), Evidence for temporal continuity of deformation in the Baltis Vallis region of Venus from observations of canali topography, *Lunar Planet. Sci.*, 31, Abstract 1692.
- Stofan, E. R., V. L. Sharpton, G. Schubert, G. Baer, D. L. Bindschadler, D. M. Janes, and S. W. Squyres (1992), Global distribution and characteristics of coronae and related features on Venus: Implications for origin and relation to mantle processes, *J. Geophys. Res.*, 97(8), 13,347–13,378.
- Sukhanov, A. L., and A. A. Pronin (1987), Evidence of tectonic spreading on Venus, *Dokl. Acad. Sci. USSR, Earth Sci. Ser.*, Engl. Transl., 294, 66–70.
- Watters, T. R. (1992), System of tectonic features common to Earth, Mars, and Venus, *Geology*, 20(7), 609–612.
- Young, D. A. (2001), Regional lineament patterns in Rusalka Planitia, *Lunar Planet. Sci. Conf.*, XXXII, Abstract 1897.
- Young, D. A., and V. L. Hansen (2003), Geological map of the Rusalka Planitia quadrangle (V-25), Venus, *U.S. Geol. Surv. Geol. Invest. Ser.*, I-2783.
- Young, D. A., L. F. Bleamaster, and V. L. Hansen (2002), Volcanism in contractional deformation belts on Venus: Evidence for point source crustal melting?, *Eos Trans. AGU*, 83, West. Pac. Geophys. Meet. Suppl., Abstract SE32C-10.
- Zuber, M. T. (1987a), Constraints on Venus' lithosphere rheology from tectonic features, *NASA Tech. Memo.*, TM-1985, 145–152.
- Zuber, M. T. (1987b), Constraints on the lithospheric structure of Venus from mechanical models and tectonic surface features, *J. Geophys. Res.*, 92(B4), 541–551.
- Zuber, M. T. (1990), Ridge belts: Evidence for regional- and local-scale deformation on the surface of Venus, *Geophys. Res. Lett.*, 17(9), 1369–1372.

V. L. Hansen and D. A. Young, Department of Geological Sciences, University of Minnesota at Duluth, 1114 Kirby Drive, Duluth, MN 55812, USA. (dyoung1@d.umn.edu)